Journal of Power Sources 248 (2014) 943–950

Contents lists available at ScienceDirect

Journal of Power Sources

journal homepage: www.elsevier.com/locate/jpowsour

A rocking chair type all-solid-state lithium ion battery adopting Li_2O–ZrO_2 coated $LiNi_{0.8}Co_{0.15}Al_{0.05}O_2$ and a sulfide based electrolyte

Seitaro Ito [a], Satoshi Fujiki [a], Takanobu Yamada [a], Yuichi Aihara [a,*], Youngsin Park [b], Tae Young Kim [b], Seung-Wook Baek [b], Jae-Myung Lee [b], Seokgwang Doo [b], Nobuya Machida [c]

[a] AR Center, Samsung R&D Institute Japan, Minoh Semba Center Bldg. 13F, Semba Nishi 2-1-11, Minoh, Osaka 562-0036, Japan
[b] Energy Storage Group, Energy Lab, SAIT, Samsung Electronics Co., LTD., San 14-1, Nongseo-Dong, Giheung-Gu, Yongin-Si, Gyeonggi-Do 446-712, Republic of Korea
[c] Department of Chemistry, Konan University, Okamoto 8-9-1, Higashinada-ku, Kobe 658-8501, Japan

HIGHLIGHTS

- Li_2O–ZrO_2 coating on NCA prevents the increment of the resistance during cycle.
- Li_2O–ZrO_2 coated NCA showed 91.7% capacity retention at 100 cycles.
- A 1 Ah class all-solid-state battery was prepared and demonstrated.

ARTICLE INFO

Article history:
Received 2 July 2013
Received in revised form
28 September 2013
Accepted 1 October 2013
Available online 15 October 2013

Keywords:
Solid state electrolyte
Solid state battery
Sulfide
Lithium ion battery
Glass ceramics

ABSTRACT

An all-solid-state lithium-ion battery (ASSB) using non-flammable solid electrolytes is a candidate for a next-generation battery. Although the excellent cycle performance and its high energy density are suggested in the literature, a practical size battery has not been appeared yet. In this paper, we have adopted a sulfide based electrolyte, Li_2S–P_2S_5 (80:20 mol%) to a rocking chair type lithium ion battery. The electrochemical cell consists of a Li_2O–ZrO_2 coated $LiNi_{0.8}Co_{0.15}Al_{0.05}O_2$ (NCA) cathode, an artificial graphite anode and the sulfide based electrolyte without any organic and inorganic liquids. The cathode charge transfer resistance is significantly reduced by the Li_2O–ZrO_2 coating. The total cell resistance of the Li_2O–ZrO_2 (LZO) coated NCA adopted cell is approximately one quarter of non-treated one. A standard type single cell with the nominal capacity of 100 mAh at 25 °C is fabricated by wet printing process, and its capacity retention is approximately 80% at 100 cycles. Also, a 1 Ah class battery was constructed by stacking the single cells, and demonstrated.

1. Introduction

Solid state lithium batteries have attracted great interest because of their high safety and applicability to EV applications and/or large scale energy storage systems. In the application of the solid electrolytes to the lithium batteries, Perovskite-type solid solution, NASICON type phosphate, garnet like structures and sulfide compounds have been studied mainly to increase their ion conductivities [1–8]. Although the performance of such solid state batteries has been reported by several groups, there are still some issues with solid-solid interfacial reaction to be overcome to enable practical usage [9–12]. For example, an oxide type electrolyte generally shows a large grain boundary resistance [13–15], and NASICON type lithium ion conductors are not stable with lithium metal, whereas the ion conductivity of such ceramic conductors have reached practical levels [16,17]. Only all-solid-state the micro-batteries, e.g., thin film type batteries based on LiPON electrolyte, fabricated by chemical vapor deposition have been commercialized and then only for memory backup and other low power usages [18,19]. From a viewpoint of a larger all-solid-state battery (ASSB), it is known that the xLi_2S–yP_2S_5 electrolyte is one of the candidates, since this kind of electrolyte shows a high ionic conductivity without a grain boundary resistance at room temperature [20,21]. The xLi_2S–yP_2S_5 electrolytes are also easily pelletized by a hand press at room temperature, and are applicable to cell assembly without a sintering process. Hence, the sulfide electrolyte is an

* Corresponding author.
E-mail address: yuichi.aihara@samsung.com (Y. Aihara).

0378-7753/$ – see front matter © 2013 Elsevier B.V. All rights reserved.
http://dx.doi.org/10.1016/j.jpowsour.2013.10.005

appropriate material for forming intimate interfacial contact with an active material, and excellent performance was achieved at the test cell scale (e.g., electrode size ~ 2 cm in diameter) [22,23].

The sulfide electrolyte also has the issue of the interface stability at the cathode. The electrolyte component atoms: sulfur, phosphorus and transition metals (cobalt, nickel and manganese), and oxygen originating from mutual diffusion, form a highly resistive layer [24]. However, others have claimed that the origin of highly resistive layer is not mutual diffusion but a Schottky barrier at the interface [25,28,32]. As yet, this is not entirely clear, surface treatment has been generally adopted to stabilize the cathode interface in sulfide based all-solid-state batteries [24–28]. Although the phenomena are different from the conventional lithium ion batteries (LIB), some of the surface coating techniques suggested in LIB is considered to be applicable to the solid-state cells [29]. Machida et al., has reported that a ZrO_2 protection layer on $LiNi_{1/3}Mn_{1/3}Co_{1/3}O_2$ is particularly beneficial [24]. In this work, the Li_2O–ZrO_2 (LZO) coating method was used to facilitate lithium ion transfer at the interface due to the existence of the Li carrier in the protection layer. However the coating layer is still expected to be resistive to ionic transport due to its low ionic conductivity, and thus the loading amount requires optimization [30].

In general, an ASSB requires external pressure to maintain fine interface contact during the charge/discharge process because the expansion/contraction of the active materials break the physical contact and increases the cell resistance during cycles. On the other hand in a conventional lithium ion battery, the liquid electrolyte and the swelled binder maintains a good interface without external pressure even if the active materials expand during the cycles. Consequently, the well-known powder compression method is unsuitable for the manufacturing process of ASSB. Thus, how to form the electrodes and electrolyte layer is another issue at this stage.

In this study, we report on the progress in developing a practical scale solid-state battery. To prevent the above issues, we have adopted three approaches: 1) an Li_2O–ZrO_2 thin layer coating was applied to the cathode material to reduce the solid–solid interface resistance and prevent mutual diffusion at the cathode/electrolyte interface. 2) A coating was applied to the electrode and electrolyte preparation. 3) A solid electrolyte free anode was adopted for avoiding contamination during the coating process and this process provided external pressure free cell operation. Together these techniques contribute to the successful operation of a practical size solid state lithium ion battery. In this report, we focus on the influence of LZO coating on NCA using a test cell, and briefly describe the characteristics of practical size single cells and the outstanding issues.

2. Experimental procedure

2.1. Preparation of the materials

For the cathode active material, an Li_2O–ZrO_2 (LZO) coated $LiNi_{0.8}Co_{0.15}Al_{0.05}O_2$ (NCA) was prepared by the sol–gel method based on ZrO_2 coating [24]. The LZO coating sol was prepared from 2-propanol (dehydrated, Kanto Chemical, Japan), lithium methoxide (equivalent of 10%-lithium methoxide in methanol solution, Kanto Chemical, Japan) and zirconium(IV) tetrapropoxide ($Zr(OC_3H_7)_4$) (TCI, Japan) in the molar ratio 200:2:1. NCA (D_{50} = ca. 5 μm) was dispersed into above solution and stirred 1 h, and the propanol evaporated under vacuum at 50 °C (water bath) while undergoing ultrasonic wave irradiation in order to prevent the NCA particles from aggregating. After filtration, the precursor was heated at 350 °C for 1 h under air, and the LZO coated NCA was prepared. After the LZO coating, the specific surface areas were verified using the nitrogen adsorption Brunauer–Emmett–Teller (BET) method (Macsorb 1208, Mountech, Tokyo). The specific surface areas of bare and LZO coated NCA were 0.45 and 0.55 $m^2\ g^{-1}$, respectively. The solid state ion conductor, amorphous Li_2S–P_2S_5 (80:20 mol%) electrolyte was prepared by high energy ball milling in accordance to the previous paper [31]. Artificial graphite (spherical shape, D_{50} = ca. 15 μm) was used for the anode active material. All the above processes were carried out in an Ar filled glove box.

2.2. Preparation of a pelletized cell

A pelletized test cell was prepared for measuring the basic characteristics such as the charge/discharge potential profiles, rated discharge capability and the cell internal resistance.

The pellet was prepared by using a die with a diameter of 13 mm as shown in Fig. 1. The test cell comprises of the stainless steel outer casing with the Teflon insulator. Then, 70 mg of the electrolyte Li_2S–P_2S_5 (80:20 mol%) powder was measured by a micro-balance and uniformly spread inside the die by a micro-spatula. Next, the powder was once temporally compressed and compacted into a pellet.

15 mg of the cathode composite powder (NCA:vapor grown carbon fiber (VF, fiber diameter = ca. 200–500 nm, length = ca. 5–10 μm):Li_2S–P_2S_5 (80:20 mol%) = 60:5:35 (wt%)) was uniformly spread across the compacted electrolyte surface in the die. Then the cathode layer was temporally hydraulically compressed. On the opposite side of the electrolyte pellet, 15 mg of the anode composite powder (artificial graphite:VF:Li_2S–P_2S_5 (80:20 mol%) = 60:5:35 (wt%)) was deposited and pelletized by the same means as the cathode layer. All the cell components were compressed together and completely pelletized by using a hydraulic press (at 25 °C, 4 ton for 30 s were applied to the 13 mm die).

After closing the upper current collector, the screw was fastened at 3.0 Nm using a preset torque wrench to maintain the electrochemical contact in the cell. The top current correct serves as the negative electrode. The upper and lower halves of the cells were electrically disconnected by an O-ring. The cell was placed in the aluminum laminated bag and vacuum sealed to avoid possible exposure of the sample to the air. All above process were carried out under Ar filled glove box (the dew point was below −70 °C).

2.3. Preparation of a practical size cell

To prepare the cathode electrode, a cathode slurry was first prepared by mixing the four components: LZO coated NCA (59wt%), Li_2S–P_2S_5 (80:20 mol%) amorphous electrolyte (34 wt%), a

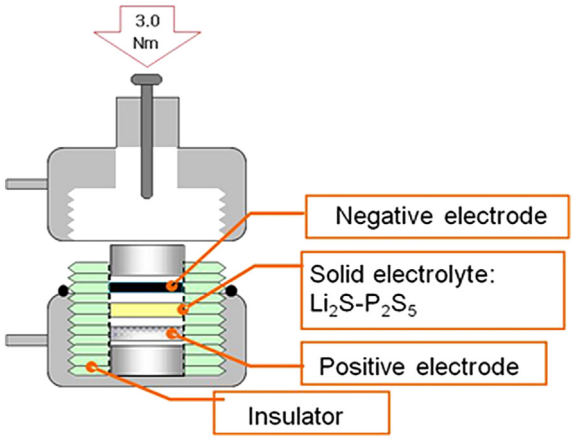

Fig. 1. Schematic structure of the test cell. The pelletized cell components are pressurized by a torque (3.0 Nm) to ensure contact. The current collectors (upper and lower vessels) are made from a stainless steel 316.

conductive carbon based on a carbon nanotube (5 wt%) and a nitrile butadiene rubber based hydrocarbon polymer binder (2 wt%) in dehydrated xylene. The slurry was used to coat carbon coated aluminum foil. After evaporation of the xylene, the electrodes were cut into predetermined shapes, and dried at 60 °C in a vacuum oven for 8 h. All processes in preparing the cathode were carried out in a dry room (dew point below −50 °C). The anode electrode was prepared from typical PVdF slurry under a normal atmosphere. The electrode was composed of 95 wt% artificial graphite and 5 wt% PVdF. A nickel current corrector was adopted for the anode. The loading levels of the electrodes were at 35 and 14 mg cm^{-2} for the cathode and anode, respectively.

The graphite anode was prepared by a conventional coating technique which has been generally adopted in the preparation process of LIBs. An artificial graphite was dispersed in PVdF (5 wt% against the graphite) dissolved dehydrated 1-methyl-2-pyrrolidone (NMP) solution. The anode slurry was coated with 10 μm thick nickel foil using a doctor blade. The electrode was dried at 60 °C for 1 h, and then dried at 80 °C under a vacuum below 0.1 torr for 18 h. A solid electrolyte layer based on Li_2S–P_2S_5 (80:20 mol%), was directly formed by coating on the surface of the graphite anode. The solid electrolyte slurry (Li_2S–P_2S_5 (80:20 mol%) dispersed in 2 wt% of hydrocarbon binder dissolved xylene solution) was coated on the anode. The reason that the conventional PVdF bonded electrode was adopted for this cell, was to maintain the separation of the anode and electrolyte at the interface, because the same binder both in anode and electrolyte layer was not applicable to the printing process due to its common solubility with xylene. Also since the sulfide electrolyte significantly reacts with NMP, sulfide electrolyte was not used for the anode side. And this absence of electrolyte in the anode consequently helps to increase the energy density.

After drying, the anode–electrolyte assembly and the cathode were placed on the opposite sides of an electrolyte layer to form a cell. The cell was then compressed together. The thicknesses of the cell components were approximately 100, 200 and 250 μm for the anode, electrolyte and cathode, respectively. The electrode active area was 88 × 53 mm^2, and three cell types were prepared: (a) single side coated, (b) both sides coated, and (c) stacked. All the cells were placed inside the aluminum laminated bag, and vacuum sealed to prevent exposure to air. The cell was designed with the following performance criteria: Positive active material = 120 mAh g^{-1}, Negative active material = 275 mAh g^{-1}, and the gross Negative/Positive capacity ratio = 1.0. The active surface area of the single side electrode is 46.64 cm^2 (restricted by cathode).

2.4. Characterization

The powder X-ray diffraction (XRD, CuKα, 45 kV, 40 mA) pattern was measured using an Empyrean XRD system (PANalytical, Almelo) for verifying the crystal structure of the Li_2O–ZrO_2 coating on NCA at room temperature. An Ar-gas-filled sample holder was used to prevent degradation due to moisture.

An SEM image was obtained using a field emission scanning electron microscopy JSM-6060 (JEOL, Tokyo). The sample was not specially treated for the SEM observation. An energy dispersive X-ray analysis (EDX) was also carried out to determine the distribution of the element. A TEM image of a cross section was observed using a transmission electron microscope, JEM-2100F (JEOL, Tokyo). The cross sectional sample was prepared by using a focused ion beam system, FB-2000A FIB (Hitachi, Tokyo).

Electrochemical impedance (EIS) was performed using an AUTOLAB PGSTAT30 (Metrohm Autolab, Utrecht) controlled by a personal computer with the cells contained in a temperature chamber, ESPEC TH-241(Espec, Osaka) with an amplitude of 10 mV in a frequency range of 0.1–1 MHz at 25 °C under a normal pressure. The EIS results were analyzed using ZSimpWin (ver. 3.21), and the correspondence of the simulated results was controlled by χ^2 (below 10^{-5}). The cycle and rate performances of the cell were measured by a battery tester, TOSCAT-3000 (Toyo system, Fukushima). The standard cut off voltages for the cycle test were set at 4.0 V and 2.5 V for charge and discharge, respectively.

3. Results and discussion

3.1. Influence of LZO coating on NCA

SEM images of bare and LZO coated NCA are shown in Fig. 2. The surface of the NCA particles appeared rounded by the LZO coating. Although it is difficult to distinguish the thickness of the LZO coated layer from the SEM picture, NCA was covered by the LZO layer. SEM-EDX analysis supports the homogeneous distribution of Zr atoms. This indicates that the Zr compound is not localized on the NCA surface by the coating process. A TEM image of a cross section of a 0.5 mol% LZO coated NCA primary particle is shown in Fig. 3. The thickness of the LZO layer for the 0.5 mol% LZO coated NCA was presumed to be around 6–8 nm, and the LZO mostly covered the NCA surface. The homogeneous LZO coating layer was obtained as an intermediate protection layer from the side reaction with sulfide electrolyte.

A powder X-ray diffraction of LZO coated sample is shown in Fig. 4. The main peaks attributed to NCA were unaltered by the LZO coating process including annealing at 350 °C. If a tetragonal Li_2O–ZrO_2 phase was formed, some peaks would be observed at position indicated by the arrow in Fig. 4(right figure). However the tetragonal Li_2O–ZrO_2 phase was not observed, since the annealing temperature was 350 °C and is too low to form the tetragonal phase.

To compare the cell performance of the bare NCA and LZO coated samples, the test cells were prepared and examined.

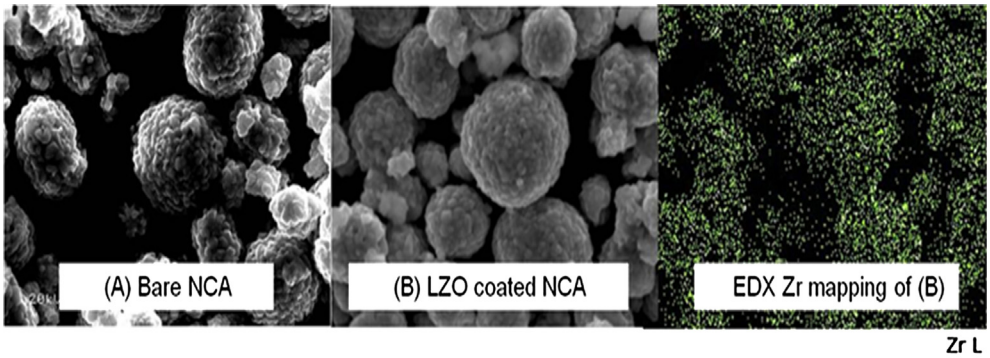

Fig. 2. SEM images of (A) bare and (B) 0.5 mol% LZO coated NCA, and corresponding EDX Zr mapping of (B). The mean particle size of NCA, D_{50} is approximately 5 μm.

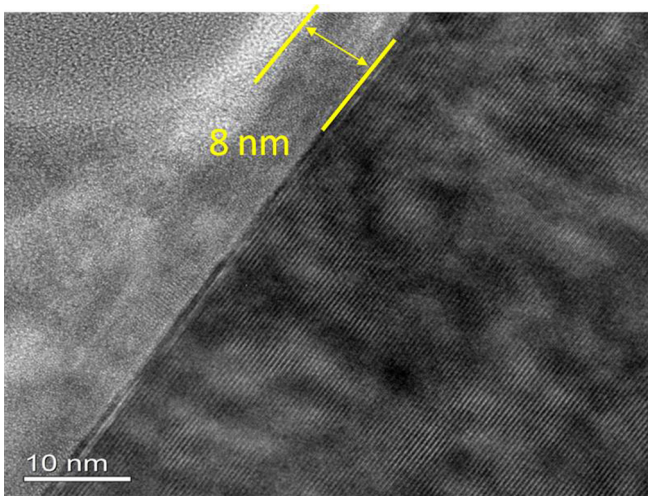

Fig. 3. A TEM image of a cross section of a 0.5 mol% LZO coated NCA particle. In the figure, the right hand (dark) side corresponds to NCA. The boundary was also verified by the elements using an EDX.

Notably, the influence of the LZO coating was found in the cathode charge transfer resistance measured by EIS after the initial charge. The results of the EIS measurement after the 1st charge (~4.0 V) are given in Fig. 5. The impedances were analyzed by a simulation based on an equivalent circuit: $LR_b(R_{ct1}Q_{ct1})(R_{ct2}Q_{ct1})W$, where the L is the inductance, R_x is the resistance, Q_y is the constant phase element, and W is Warburg diffusion. Here, R_b indicates the bulk resistance corresponding to the Ohmic drop which is mostly attributed to the ion conductivity of the electrolyte, and R_{ct1} and R_{ct2} indicate the charge transfer resistances of the anode and the cathode, respectively. To obtain better fitting parameters, several points attributed to the capacitance given in the solution resistance in the high frequency region (above 100 kHz) were neglected. The fitting results are shown in Fig. 5(B), and the separate resistance for each component is given in Table 1. It is certain that the cathode charge transfer resistance, R_{ct2}, is the largest resistive component in the total cell resistance, though we cannot clearly state whether the anode impedance is sufficiently small in comparison with the cathode side or not. The reason that the cathode impedance comprises most of the resistance in our cell may be due to the side reaction between sulfide electrolyte and cathode at the interface, especially for bare NCA. The anode R_{ct1} is around half that of the cathode. However, the utilization of the anode (i.e., the same weight of the graphite is used for these test cells to evaluate the cathode) must be taken into account when considering the relative value of the anode impedance. The minimum impedance was obtained at 0.5 mol% LZO coating. Whereas a 1.5 mol% LZO coating increased the resistance in comparison with a 0.5 mol% LZO coating. The thick coating layer (i.e., 1.5 mol% LZO coat) might obstruct the charge transfer at the cathode/electrolyte interface, because the ionic conductivity of Li_2O–ZrO_2 should be lower than that of the sulfide based electrolyte [30]. If the thickness of the LZO layer is sufficient to carry out the charge transfer process, it can be assumed that the LZO layer suppresses the following resistive components: (1) a resistance originating in the mutual diffusion layer formed by the side reaction between sulfide and NCA (oxide), and (2) a resistance originating in the poorly electrochemical active surface between the NCA and the electrolyte. The former phenomenon is well-known in the sulfide system [24–28]. The latter is not generally observed in conventional LIBs due to the penetration of the liquid electrolyte into micro pores. In fact, the physical formation of the interface is a significant issue in all solid systems, because a sufficiently active surface cannot be easily fabricated through solid–solid contact. The physical specific surface area of NCA increased upon coating with the LZO (the exact values are given in the Experimental Section, the specific surface area of LZO coated NCA is approximately 120% of the bare NCA.). Since the LZO layer covers the micro pores, i.e., LZO covers primary and secondary particles at the nano level (see TEM image in Fig. 3), the physical contacting surface area between LZO and NCA must be much larger than that of the sulfide electrolyte/NCA. At the present stage, we presume (1) the LZO layer (approximately 8 nm thick) does not behave as an obstruction for the net electrochemical reaction, and protects the NCA surface from the side reaction with sulfide. However, a thick LZO layer behaves as an obstruction because of the slow lithium ion diffusion in the LZO. (2) The enlarged physical surface area probably affects the impedance. However, the effect must be limited, since the enhancement of the physical surface area does not significantly alter the impedances, and (3) since the lithium ion diffusion in LZO must be much slower than in Li_2S–P_2S_5 and NCA, the surface coverage of LZO does not significantly influence the effective electrochemical active surface. Therefore, the small impedance given in the LZO coated NCA may be caused of the protection from the side reaction at initial charge rather than the increase of the electrochemical active surface by LZO surface coverage.

The rated performance of the full cells is shown in Fig. 6. Since the cell impedance of the bare NCA was much higher than the coated samples, the capacity was lower than other cells (103 mAh g^{-1}). Especially, at the high discharge rate of 1 mA cm^{-2}, the cell operating potentials were totally different to each other. The tendency of the rate capability was reflected by the charge transfer resistance (0.5 mol% coated > 1.0 mol% coated > 1.5 mol%

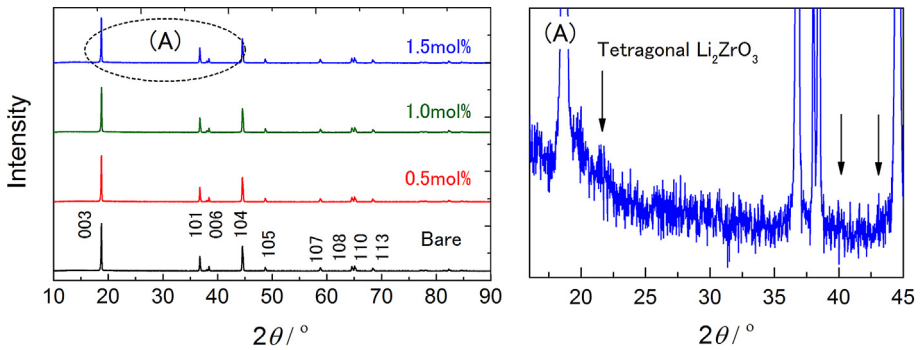

Fig. 4. XRD patterns for the bare and the LZO coated NCA with different amounts of coating. The right figure shows an extended scale within 15–45° for the 1.5 mol% LZO coated NCA (region (A) in the left side figure).

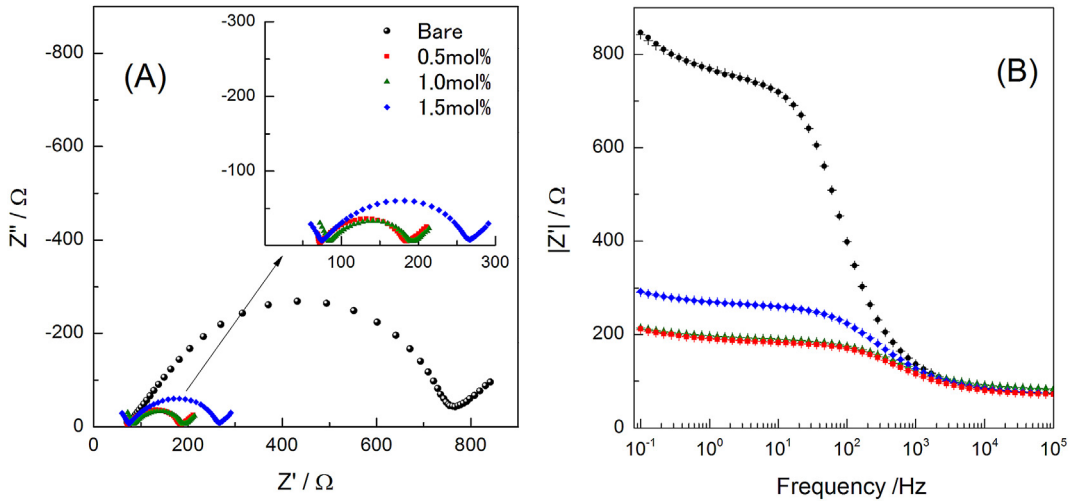

Fig. 5. Impedance of the test cells at the initial charged (bare NCA (●), and 0.5 mol% (■), 1.0 mol% (▲) and (◆) 1.5 mol% LZO coated NCA). (A) Nyquist plot and (B) Bode plot. The Bode plot contains data simulated data using an equivalent circuit (+). As can be seen the experimental data and simulations are almost perfectly overlapped.

coated >> bare NCA). The cycle performance was verified for bare and 0.5 mol% coated NCA at 0.1C charge/discharge cycle at 25 °C. The results are given in Fig. 7. The capacity retentions were 73.9 and 91.7% against the initial capacity after 100 cycles, for bare and 0.5 mol% LZO coated, respectively. It is clear that the cell capacity was well maintained in the 0.5 mol% LZO coated NCA cell in comparison with the non-treated one. A summary of the separate resistive components derived from EIS measurements at 100 cycles are shown in Table 2. Although the R_{ct1} value in both cells also increased with the cycle number, the cathode impedances (R_{ct2}) given in the bare NCA significantly increased in comparison to the 0.5 mol% LZO coated NCA after 100 cycles. To investigate some more details of the capacity decay due to R_{ct2}, EIS measurements were performed every 10 cycles for both cells until 40 cycles, and were independently performed from the above cycle test under the same test conditions. The cathode charge transfer resistance, R_{ct2} is plotted versus cycle number in Fig. 8. The resistance linearly increased in both cells, and the slope given in bare NCA was much larger than that of 0.5 mol% LZO coated NCA. Even in the LZO coated cell, the increment of the resistance was not completely prevented. However, the influence of the LZO coating was clearly verified. The increased impedance may be due to the particular reaction in sulfide system, i.e., a resistive layer formation due to the mutual diffusion of atoms at the electrolyte/cathode oxide interface [32]. Since the cathode resistance was well maintained by the LZO coating, the cathode potential could be well controlled. On the contrary, the cathode impedance increased with the cycle in the bare NCA, because the degradation of the cathode/electrolyte interface was enhanced without LZO layer at every cycles. Although the actual independent cathode and the anode potentials are unclear during the operation of the two electrode cell in this study, it is sure that suppression of the degradation reaction is strongly required to maintain the cathode potential for the sulfide based solid state battery system.

Table 1
Independent resistive components analyzed using an equivalent circuit.

	Resistance/Ω		
	R_b	R_{ct1}	R_{ct2}
0 mol% (bare)	69.7	105	247
0.5 mol% LZO coated	79.0	41.9	88.3
1.0 mol% LZO coated	71.1	20.6	98.9
1.5 mol% LZO coated	69.6	47.2	146

3.2. Demonstration performance of a practical size

Since the test cell showed a good cell performance, a card size cell was prepared by typical wet process. Indeed, if we can directly prepare a large area electrode from a composite powder, the cell performance could be used to estimate in comparison with the wet

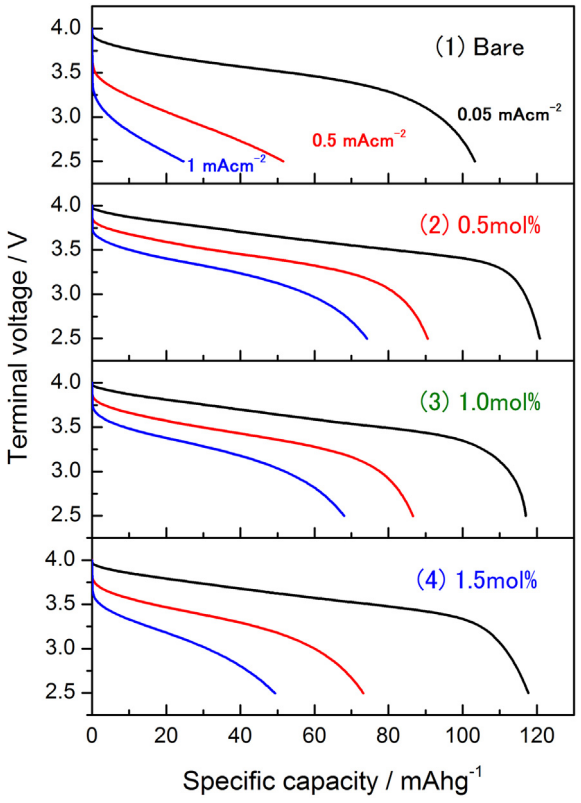

Fig. 6. Discharge rate performances of the test cells adopting (1) bare NCA, (2) 0.5 mol % LZO coated NCA, (3) 1.0 mol% LZO coated NCA and (4) 1.5 mol% LZO coated NCA, for the cathode active material. The charge rate was fixed at 0.05 mA cm^{-2}.

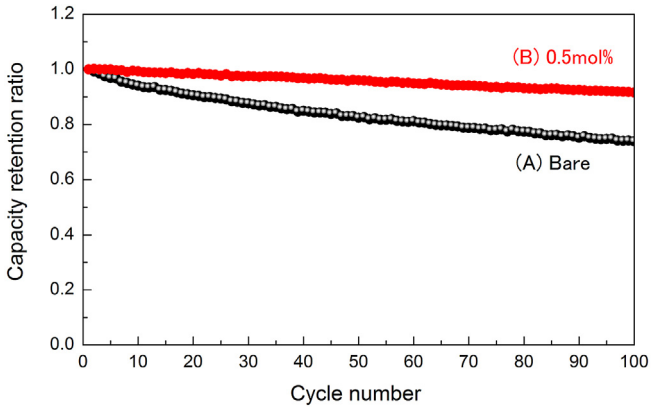

Fig. 7. Cycle characteristic of (A) bare and (B) 0.5 mol% LZO coated NCA at 25 °C. The test conditions are 0.1C constant current (CC) - constant voltage (CV) charge/0.1C constant current (CC) discharge, and the cut off potentials are 4.0 and 2.5 V for the charge and the discharge, respectively.

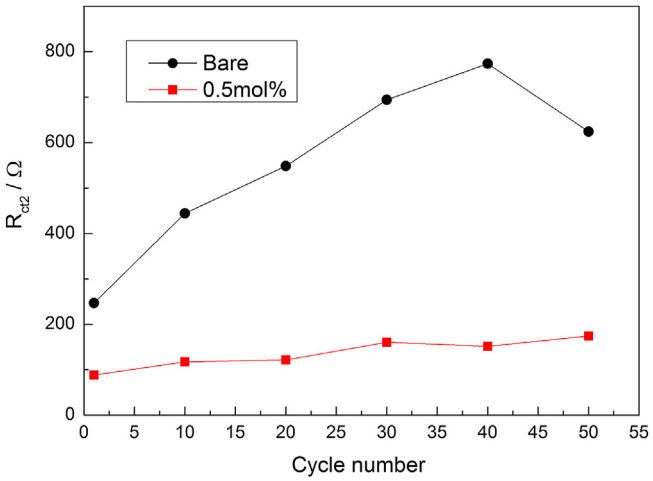

Fig. 8. Charge transfer resistance, R_{ct2} plotted versus cycle for the test cells using bare NCA (●), and 0.5 mol% LZO coated NCA (■) at 25 °C. The R_{ct2} is derived from the simulation using the equivalent circuit given in Section 3.1.

process, because we do not need to account for the resistance of the binder in the total cell resistance. On the contrary, there is a large benefit in using the binder for the fabrication process, because the conventional LIB process can be applied to prepare the solid state cell. Although there are several methods, here we adopted the simple wet process.

The microstructure of the fabricated cell was investigated using SEM and an image of a cross section of the electrode assembly is shown in Fig. 9. The thickness of the anode, the solid electrolyte and the cathode were approximately 100, 200, and 250 μm, respectively, for a 100 mAh standard single cell. In Fig. 8, the contrast of the picture and the particles' shapes may help to recognize the layered structure of the electrode assembly. In fact, the solid electrolyte layer is very thick compared to a PE separator (below 30 μm in general) adopted in LIBs. However, the thick layer was prepared only for preventing the short circuit, because the electrolyte was directly coated on the anode. To ensure separation between the cathode and anode, a thick electrolyte layer is needed. In this preparation process, an important step was to use the PVdF binder for the anode. The electrolyte slurry based on xylene could be easily coated on the anode side without mutual dissolution of each layer at the interface. If the same binder is adopted for both the electrode and electrolyte layer, it is impossible to prepare the electrolyte layer directly on the electrode due common solubility of the binder by the wet process. However, this problem could be completely solved, since PVdF is insoluble in xylene. Also, this gives a large benefit in the manufacturing process, because a general anode used in LIB is available for application. The external overview of the demonstration cell is shown in Fig. 10. The nominal capacity of the cell can be easily controlled by a combination of the electrode coating process and the number of parallel stacks. The cell shown in Fig. 10 has both sides coated and contains three single cells. The discharge curves of the two types of single cells and the stacked cell are shown in Fig. 11. Although the electrolyte free anode was used in the cells, the designed discharge capacity (120 mAh g^{-1} for the LZO coated NCA under a charge cut off potential of 4.0 V by a constant current) was obtained without an external artificial pressure. The cell kinetics is still governed by the cathode charge transfer resistance. The anode resistance can be negligible, though the electrolyte free anode was adopted. This is probably due to the cathode kinetics being much slower than the mass transport process in the anode.

The discharge curves related to the cycle performances for the single cells at 25 °C and 60 °C are given in Fig. 12. Indeed, the polarization is larger than the test cell as shown in Fig. 6. It is presumed that (1) the binder obstructs the ionic and/or electric conduction in the electrodes and (2) the charge transfer resistance of the solid electrolyte free anode is higher than the test cell. The designed capacity is exactly the same in both cells tested in 25 and 60 °C. However, the cell capacities were approximately 110 mAh and 125 mAh at 25 and 60 °C, respectively, due to the cell over potential. On the other hand, the capacity retention was almost the

Table 2
Resistances after 100 cycles for LZO coated and non-treated (bare) NCA and the ratio in comparison with the initial values (given in Table 1).

	Bare NCA			0.5 mol% LZO		
	R_b	R_{ct1}	R_{ct2}	R_b	R_{ct1}	R_{ct2}
R_x at 100 cycles/Ω	71.5	321	1419	82.5	125	232
Ratio (100th/init.)	1.03	3.06	5.74	1.04	2.98	2.63

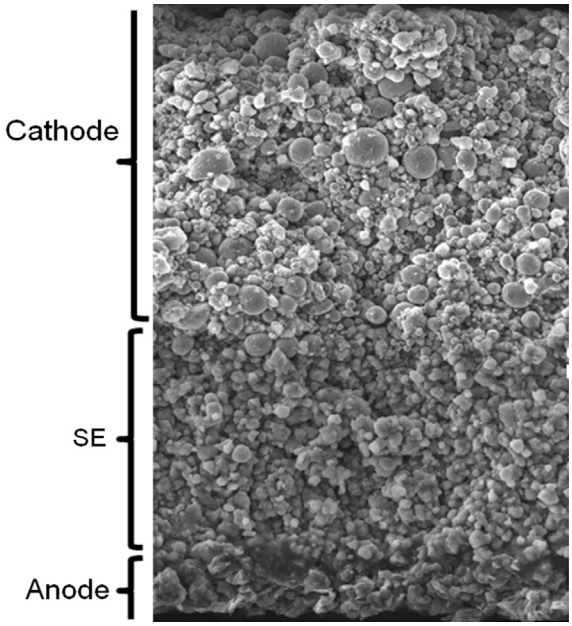

Fig. 9. Cross sectional view of the electrode assembly for a single cell coated on both sides. In the figure, "SE" indicates the solid electrolyte layer.

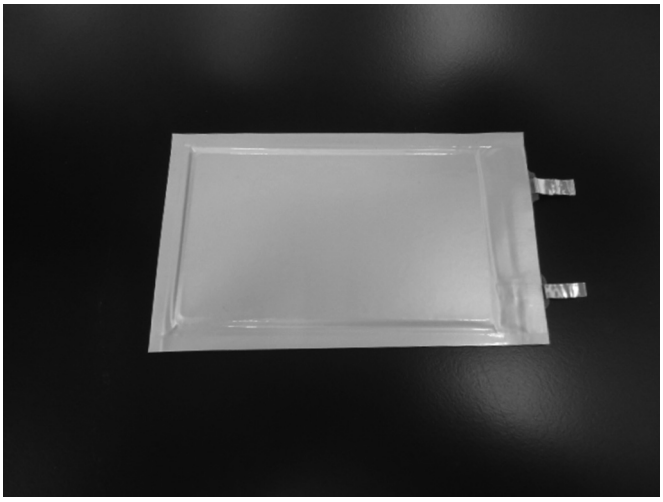

Fig. 10. The 1 Ah class demonstration cell. The cell consists of three parallel stacks of the single cells (coated on both sides).

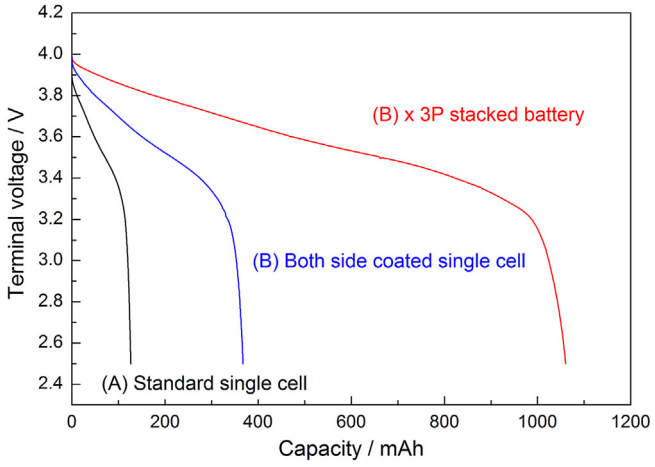

Fig. 11. 0.1C Discharge curves of (A) a single cell (single side coated), (B) a single cell (both sides coated) and (c) stacked battery (three parallel stacks of (B)) at 25 °C.

same in spite of the temperature differences. The capacity retentions at 100 cycles were 82 and 85% of initial capacities at 25 and 60 °C, respectively. This strongly indicates the high temperature stability of the all-solid-state battery, and so that the cell will be appropriate for the electric vehicle (EV) and energy storage system (ESS) applications.

Although further development is still required to improve the energy density and rate capability, the applicability of the sulfide based electrolyte to practical size lithium ion batteries was clearly demonstrated indicating the great possibility for use as a next generation battery.

4. Conclusion

A Li_2O–ZrO_2 (LZO) coating layer was prepared on a $LiNi_{0.8}Co_{0.15}Al_{0.05}O_2$ (NCA) surface to apply to sulfide based solid state battery. In a rocking chair type small test cell, 85% capacity retention at 100 cycles and good rate capability were verified. Although the mechanism of LZO protection layer is still not sufficiently understood in this study, it is presumed that the interface between the sulfide electrolyte and the NCA is maintained by the LZO layer during the cell operation, because the increment ratio of R_{ct2} during cycle is significantly reduced by the existence of the LZO layer, and a

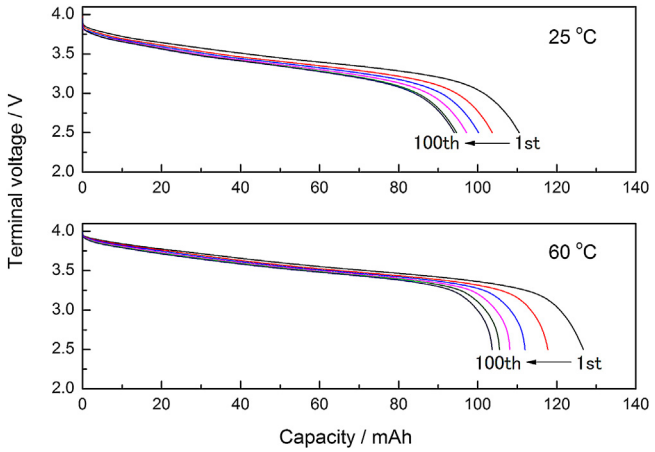

Fig. 12. Discharge curves of a single cell at 25 and 60 °C at various cycles. The discharge curves are given at every 20 cycles until 100 cycles.

thicker LZO layer indicates a higher impedance with a lower increment ratio of the impedance during the cycle.

To realize a practical size solid state battery, we have verified the possibility of fabrication of a 1 Ah class pure solid state battery without any liquid. The battery cycle performance and 80% capacity retention was verified at 100 cycles without any artificial external pressure. Although the cell performance is still not sufficient for EV application, the development is certainly progressing towards a practical size battery.

Acknowledgments

The authors express their sincere thanks to Prof. W. S. Price, University of Western Sydney and Dr. H. Visbal and Dr. T. Watanabe, Samsung R&D Institute of Japan for improving the manuscript.

References

[1] S. Stramare, V. Thangadurai, W. Weppner, Chem. Mater. 15 (2003) 3974–3990.
[2] J.S. Thokchom, N. Gupta, B. Kumar, J. Electrochem. Soc. 155 (2008) A915–A920.
[3] J.B. Goodenough, H.Y.-P. Hong, J.A. Kafalas, Mater. Res. Bull. 11 (1976) 203–220.
[4] H.Y.-P. Hong, Mater. Res. Bull. 13 (1978) 117–124.
[5] M.A. Subramanian, R. Subramanian, A. Clearfield, Solid State Ionics 18&19 (1986) 562–569.
[6] H. Aono, E. Sugimoto, Y. Sadaoka, N. Imanaka, G. Adachi, J. Electrochem. Soc. 136 (1989) 590–591.
[7] R. Murugan, V. Thangadurai, W. Weppner, Angew. Chem. Int. Ed. 46 (2007) 7778–7781.
[8] M. Tatsumisago, F. Mizuno, A. Hayashi, J. Power Sources 159 (2006) 193–199.
[9] Shingo Ohta, Tetsuro Kobayashi, Juntaro Seki, Takahiko Asaoka, J. Power Sources 202 (2012) 332–335.
[10] Masashi Kotobuki, Kiyoshi Kanamura, Ceram. Int. 39 (2013) 6481–6487.
[11] Ying Jin, Paul J. McGinn, Electrochim. Acta 89 (2013) 407–412.
[12] Kazunori Takada, Noboru Aotani, Kazuya Iwamoto, Shigeo Kondo, Solid State Ionics 86-88 (1996) 877–882.
[13] Chinnasamy R. Mariappan, Michael Gellert, Chihiro Yada, Fabio Rosciano, Bernhard Roling, Electrochem. Commun. 14 (2012) 25–28.
[14] H. Aono, E. Sugimoto, Y. Sadaoka, N. Imanaka, G. Adachi, Chem. Lett. (1990) 331–334.
[15] H. Aono, E. Sugimoto, Y. Sadaoka, N. Imanaka, G. Adachi, J. Electrochem. Soc. 137 (1990) 1023–1027.
[16] Nobuyuki Imanishi, Satoshi Hasegawa, Tao Zhang, Atushi Hirano, Yasuo Takeda, Osamu Yamamoto, J. Power Sources 185 (2008) 1392–1397.
[17] K. Nagata, T. Nanno, J. Power Sources 174 (2007) 832–838.
[18] C. Lethien, M. Zegaoui, P. Roussel, P. Tilmant, N. Rolland, P.A. Rolland, Microelectronic Eng. 88 (2011) 3172–3177.
[19] B. Fleutot, B. Pecquenard, F. Le Cras, B. Delis, H. Martinez, L. Dupont, D. Guy-Bouyssou, J. Power Sources 196 (2011) 10289–10296.
[20] M. Tatsumisago, S. Hama, A. Hayashi, H. Morimoto, T. Minami, Solid State Ionics 154–155 (2002) 635–640.

[21] K. Hayamizu, Y. Aihara, Solid State Ionics 238 (2013) 7–14.
[22] Tsutomu Minami, Akitoshi Hayashi, Masahiro Tatsumisago, Solid State Ionics 177 (2006) 2715–2720.
[23] Kazunori Takada, Taro Inada, Akihisa Kajiyama, Hideki Sasaki, Shigeo Kondo, Mamoru Watanabe, Masahiro Murayama, Ryoji Kanno, Solid State Ionics 158 (2003) 269–274.
[24] Nobuya Machida, Junji Kashiwagi, Muneyuki Naito, Toshihiko Shigematsu, Solid State Ionics 225 (2012) 354–358.
[25] K. Takada, Acta Mater. 61 (2013) 759–770.
[26] N. Ohta, K. Takada, L.-Q. Zhang, R.-Z. Ma, M. Osada, T. Sasaki, Adv. Mater. 18 (2006) 2226–2229.
[27] Atsushi Sakuda, Akitoshi Hayashi, Masahiro Tatsumisago, J. Power Sources 195 (2010) 599–603.
[28] Yoshikatsu Seino, Tsuyoshi Ota, Kazunori Takada, J. Power Sources 196 (2011) 6488–6492.
[29] C. Li, H.P. Zhang, L.J. Fu, H. Liu, Y.P. Wu, E. Rahm, R. Holze, H.Q. Wu, Electrochim. Acta 51 (2006) 3872–3883.
[30] E.E. Hellstrom, W. Van Gool, Solid State Ionics 2 (1981) 59–64.
[31] Marco Agostini, Yuichi Aihara, Takanobu Yamada, Bruno Scrosati, Jusef Hassoun, Solid State Ionics 238 (2013) 7–14.
[32] N. Ohta, K. Takada, I. Sakaguchi, L. Zhang, R. Ma, K. Fukuda, M. Okada, T. Sasaki, Electrochem. Commun. 9 (2007) 1486–1490.